Submesoscale cyclones in the Agulhas current

M. Krug, S. Swart, J. Gula

AGU PUBLICATIONS

Geophysical Research Letters

RESEARCH LETTER
10.1002/2016GL071006

Key Points:
- Glider observations show the presence of submesoscale cyclonic eddies at the inshore boundary of the Agulhas Current
- Submesoscale cyclones are generated through shear instability of the current
- Submesoscale cyclones drive warm water plumes towards the continental shelf

Supporting Information:
- Supporting Information S1

Correspondence to:
M. Krug,
mkrug@csir.co.za

Citation:
Krug, M., S. Swart, and J. Gula (2017), Submesoscale cyclones in the Agulhas current, *Geophys. Res. Lett.*, *44*, 346–354, doi:10.1002/2016GL071006.

Received 30 AUG 2016
Accepted 31 DEC 2016
Accepted article online 5 JAN 2017
Published online 14 JAN 2017

Submesoscale cyclones in the Agulhas current

M. Krug[1,2], S. Swart[3,4,5], and J. Gula[6]

[1]Ecosystem Earth Observation, CSIR, Stellenbosch, South Africa, [2]Department of Oceanography, Nansen-Tutu Center for Marine Environmental Research, University of Cape Town, Cape Town, South Africa, [3]Southern Ocean Carbon and Climate Observatory, CSIR, Stellenbosch, South Africa, [4]Department of Oceanography, University of Cape Town, Cape Town, South Africa, [5]Now at Department of Marine Sciences, University of Gothenburg, Gothenburg, Sweden, [6]Univ. Brest, CNRS, IRD, Ifremer, Laboratoire d'Océanographie Physique et Spatiale (LOPS), IUEM, Brest, France

Abstract Gliders were deployed for the first time in the Agulhas Current region to investigate processes of interactions between western boundary currents and shelf waters. Continuous observations from the gliders in water depths of 100–1000 m and over a period of 1 month provide the first high-resolution observations of the Agulhas Current's inshore front. The observations collected in a nonmeandering Agulhas Current show the presence of submesoscale cyclonic eddies, generated at the inshore boundary of the Agulhas Current. The submesoscale cyclones are often associated with warm water plumes, which extend from their western edge and exhibit strong northeastward currents. These features are a result of shear instabilities and extract their energy from the mean Agulhas Current jet.

1. Introduction

The Agulhas Current (AC) is the strongest western boundary current (WBC) of the Southern Hemisphere, with an average transport of 70 sverdrup and current speeds in excess of 2 m s^{-1} [*Beal et al.,* 2011]. As it flows southward along the continental shelf break, the AC influences the oceanography of coastal and shelf regions through a range of mesoscale (~50–200 km) and submesoscale (<10 km) processes, such as eddy shedding, plumes, filaments, and the intrusion of the current onto the shelf during meandering [*Lutjeharms*, 2006; *Krug et al.,* 2014]. Most studies documenting the dynamics at the AC front have focused on large solitary meanders or so-called Natal Pulses (50–200 km in diameter) produced by barotropic instabilities and associated with a northeastward flow at the shelf break and strong upwelling at their leading edge [*Beal and Bryden,* 1999; *Elipot and Beal,* 2015; *Pivan et al.,* 2016]. Smaller mesoscale cyclonic eddies, about 50 km in diameter, have been observed along the Agulhas Bank, south of 34°S. They have no linkage to Natal Pulses and have been labeled frontal eddies [*Schumann and van Heerden,* 1988] or shear edge eddies [*Lutjeharms et al.,* 1989]. Submesoscale cyclonic eddies (about 10 km in diameter) have also been observed in the wake of mesoscale meanders [*Lutjeharms et al.,* 2003]. Characterizing the impact of smaller mesoscale or submesoscale cyclones has proved difficult due to their short residence time and the very limited number of observations available. *Lutjeharms et al.* [2003] found no evidence that they induced upwelling on the shelf, and more generally, the impact of these smaller cyclones on the mean cross-shelf structure remains uncertain.

In April 2015, two Seagliders were deployed for the very first time in the AC region as part of the Shelf Agulhas Glider Experiment (SAGE). The profiling gliders offered a state-of-the-art technology to sample the energetic inshore regions of the AC by providing continuous measurements of the water column at high spatial (100 s of meters to 3 km—well within the submesoscale range) and temporal (0.5–4 hourly) resolution. Our observations provide new insight on the properties and dynamics of the AC front. After describing our data set and method (section 2), we characterize the dynamical processes observed at the inshore edge of a nonmeandering AC (section 3) before concluding on our results (section 4).

2. Materials and Methods

2.1. Seaglider Acquisitions and Processing

Seagliders are buoyancy-driven autonomous underwater vehicles. A set of wings, coupled with a low-drag hydrodynamic shape, drives forward propulsion as the glider samples a range of parameters between the surface and 1000 m depth. Measured variables are communicated back via satellite in real time, while the glider functioning is controlled by pilots on land [*Eriksen et al.*, 2001; *Rudnick*, 2016]. Seagliders SG543 and

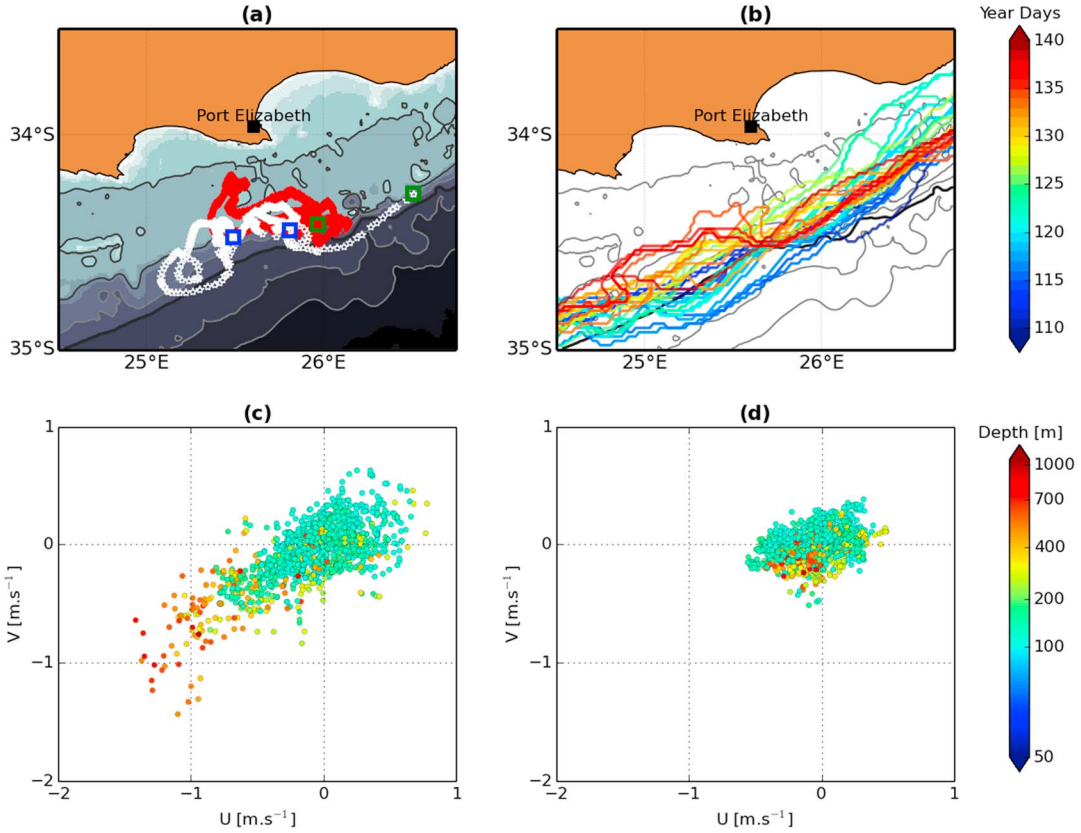

Figure 1. (a) Glider trajectories between year days 109 and 140. Deployment and recovery positions are plotted with green and blue squares, respectively. The gray color scale shows the bathymetry with darker tones toward the deeper regions and is overlaid with the 100 m, 200 m, 500 m, 1000 m (thick black line), 2000 m, and 3000 m isobath contours. (b) Location of AC inshore edge derived from the Odyssea SST between year days 109 and 140. The color bar represent days in 2015. Scatterplots of the *U* and *V* components of the flow observed from both gliders for (c) surface and (d) depth-averaged currents. The color bar associated with all markers in Figures 1c and 1d indicates the water depth for each dive.

SG573 were deployed off Africa's southeastern shores, near 34°S, 26°E (Figure 1a). The gliders were initially directed along cross-shore transects running between the 100 m and 1000 m isobaths offshore Algoa and Cape St. Francis Bays to study interactions between the AC and the coast. Strong currents provided challenges to the planned experiment design, and the observational strategy was adjusted accordingly to maximize sampling between the AC inshore front and the continental shelf.

On each dive, the gliders collected conductivity-temperature-depth (CTD) data at an average rate of two acquisitions per meter. CTD sensors on board the gliders were calibrated using ship-based CTD casts and salinity bottle samples collected during deployment and recovery. Only the downcast CTD data are presented here as it shows less spread in temperature/salinity space. All CTD data were gridded to a 1 m vertical resolution and subjected to a spike and gradient test following the procedures defined in *Wong et al.* [2009]. For each glider dive, depth- (and time-) averaged currents were estimated by comparing GPS-measured displacement to through-water displacement estimated from a Seaglider flight model. Surface currents were estimated from the gliders' surface drift. Uncertainties in current speed estimates for the Seagliders are of the order of ~0.01 m s^{-1} for the depth averaged current [*Eriksen et al.*, 2001] and are estimated to be ~0.05 m s^{-1} for the surface currents using the distance between successive GPS fixes at the surface and a 10 m GPS fix accuracy. The surface current velocity data set was then subjected to additional quality control, whereby data points with total, eastward, or northward velocity exceeding their 3 h moving median by 1 m s^{-1} were flagged as outliers and removed. The surface current velocities presented here consist of 3 h moving medians of the quality controlled time series. The duration of the gliders dives varied between 20 min and 6.7 h with most dives lasting about 1 h. Along-shore velocities refer to currents rotated 45° from north, in line with the mean AC direction and the general direction of the 1000 m isobath.

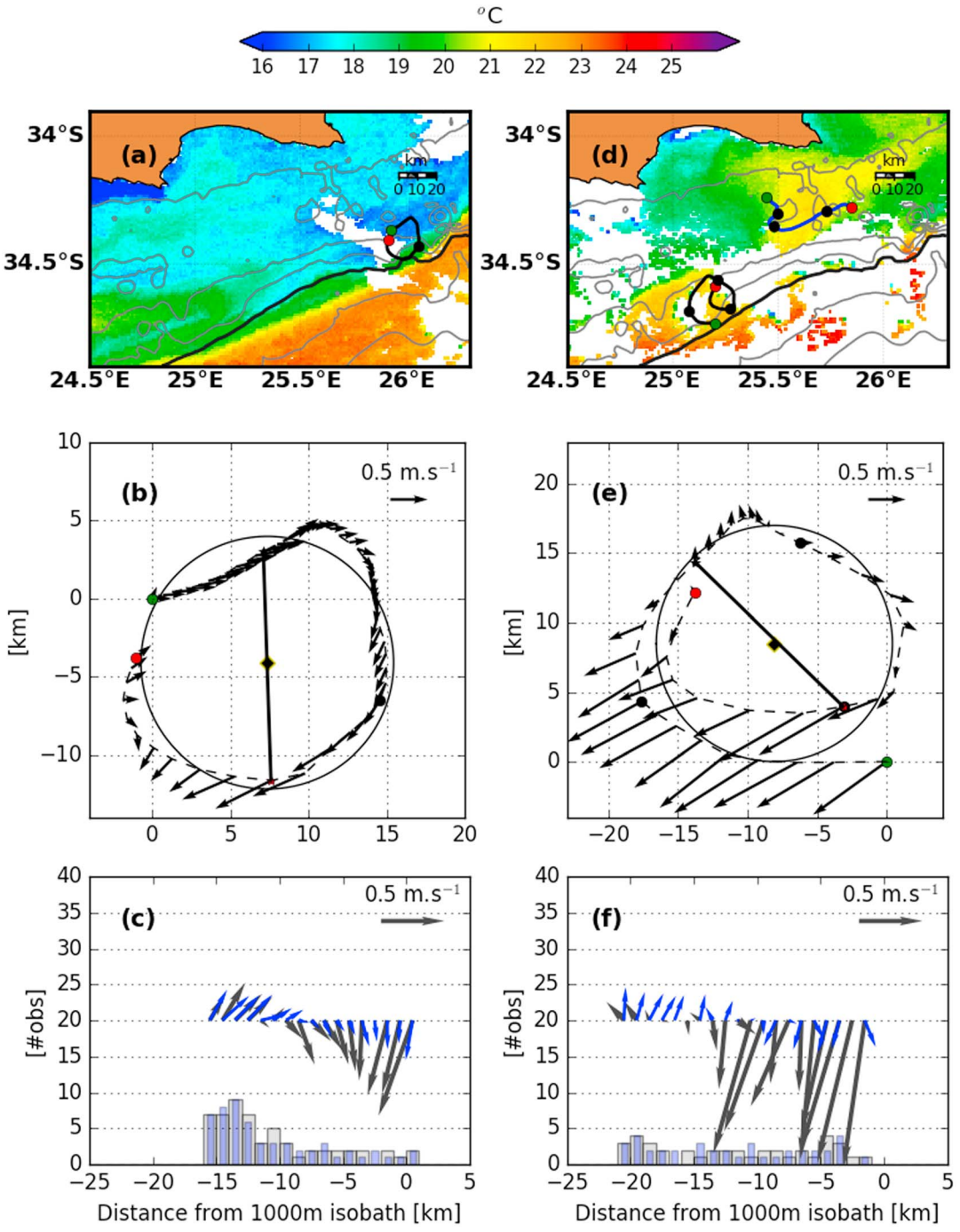

Figure 2. Selected case studies of submesoscale cyclones. (a–c) Data collected from SG543, between day 110 and 113, and (d–f) data from SG573, between day 134 and 137. Figures 2a and 2d show the path of the gliders overlaid on MODIS SST maps. Gray contours show the locations of the 100 m, 200 m, 500 m, 1000 m (thick black line), 2000 m, and 3000 m isobaths. Green and red dots mark the start and end position of the gliders with each black dot marking daily intervals. In Figure 2d, the path of SG543 was added in blue. Figures 2b and 2e show the spatial extent (in km) and flow magnitude (in m s^{-1}) for the submesoscale cyclones. Note that the mean drift of glider SG573 in the cyclonic eddy has been removed in Figure 2e. Figures 2c and 2f show a cross-shelf representation of the cyclones with vectors indicating surface (black) and depth-averaged (blue) currents. The currents in Figures 2c and 2f are rotated 45° from north so that vectors pointing directly upward indicate a flow toward the northeast. Histograms show the number of valid observations with the number counts on the left-hand side *Y* axis.

2.2. Satellite Data Sets and Analysis

Odyssea gridded maps of merged sea surface temperature (SST) were used to follow perturbation at the AC front using the method described in the supporting material. The Odyssea product is provided at daily intervals and a spatial resolution of 2 km. Daytime composites of SST from the Moderate Resolution Imaging Spectroradiometer (MODIS) aboard NASA's Aqua satellite were used in selected case studies of frontal instabilities. The MODIS data set has a 1 km spatial resolution. Wind stress was computed using the National Centers for Environmental Prediction (NCEP) Climate Forecast System Version 2 (CFSv2) hourly time series 10 m wind product [*Saha et al.,* 2014] and the *Yelland and Taylor* [1996] drag coefficients. The GEBCO_2014 bathymetry, available on a 30 arc sec interval grid, was used for all map plots (http://www.gebco.net).

The data presented here were collected between 19 April and 20 May 2015 (from year days 109 to 140) to depict conditions experienced at the inshore edge of the AC during a nonmeandering state.

3. Results and Discussion

3.1. Properties of the AC Front During SAGE

Analyses conducted on satellite observations of sea surface height (Figure S1 in the supporting information) and SST (Figure 1b) show that no mesoscale AC meanders were present during the study, i.e., the AC was in a nonmeandering state. During SAGE, the northern wall of the AC was generally located near the 1000 m isobath, in agreement with *Rouault et al.* [2010]. Most gliders observations were collected at the AC edge and in a region of strong topographic gradient (Figure 1a).

Observations showed an energetic and rapidly varying flow field. Depth-averaged currents had average speeds of 0.2 m s^{-1} and maximum speeds of about 0.6 m s^{-1}. Surface currents were considerably stronger, averaging 0.4 m s^{-1} and reaching maximum values of 1.8 m s^{-1}. The strongest surface currents were toward the southwest and observed in deep waters, where the gliders approached the AC (Figures 1c and 1d). There was a strong polarity in the flow direction with the principal component of the current aligned along a northeast/southwest axis and accounting for 89% and 73% of the explained variance for the surface and depth-averaged flows, respectively. A surprising result was the relatively large proportion of northeasterly flow (in a direction opposite to that of the AC flow). The currents were toward the northeast 44% of the time at the surface and 53% of the time in the depth-averaged record. More than 80% of the northeasterly flow occurred in water depths shallower than 200 m, near the shelf break.

3.2. Submesoscale Cyclonic Eddies Observations

The first instance of northeasterly flow was observed from SG543, when soon after deployment at the AC edge, the glider started to move in a northeasterly direction, away from its intended waypoint. The trajectory followed by SG543 (Figure 2a) was unexpected as no Agulhas plume or meander could be observed in the SST imagery to suggest that SG543 would move counter to the mean direction of the AC. During that period, SG543 was caught in a submesoscale cyclone with a rotation period of about 2 day and a diameter of 15 km (Figure 2a). The eddy's major axis was oriented in a southwesterly/northeasterly direction, in line with the mean AC direction. The eddy was characterized by an asymmetrical velocity structure typical of that of frontal eddies in WBC systems [*Lee et al.,* 1981; *Gula et al.*, 2016a]. In the offshore arm of the eddy, surface current velocities peaked at 0.8 m s^{-1}, whereas in the inshore arm of the eddy the maximum current velocities were about 0.4 m s^{-1} (Figures 2b and 2c). Such differences between the inshore and offshore regions of the cyclonic eddy translate to a relative vorticity value $\zeta = 1.02f$ (with f the Coriolis parameter). This estimate of ζ is comparable to that reported for large meanders of the AC [*Pivan et al.,* 2016] or Gulf Stream frontal eddies [*Brooks and Bane,* 1981]. Depth-averaged currents were of similar magnitude in both the inshore and offshore regions of the eddy (Figure 2c) despite a threefold increase in water depth on the offshore side.

A further case of countercurrent at the AC inshore front was observed between days 134 and 138, at a time when SG573 experienced two full cyclonic revolutions slightly inshore of the 1000 m isobaths (Figure 2d). Between day 134 and 138, SG573 progressed over a very steep and narrow section of the continental shelf, in water depths ranging between 150 m and 700 m (Figure 3b). The spatial extent of the eddy-like motions were slightly greater than in the previous case but still within the submesoscale range since the Rossby radius of deformation in our study region is between 30 and 40 km [*Chelton et al.,* 1998]. The cyclonic eddy had a

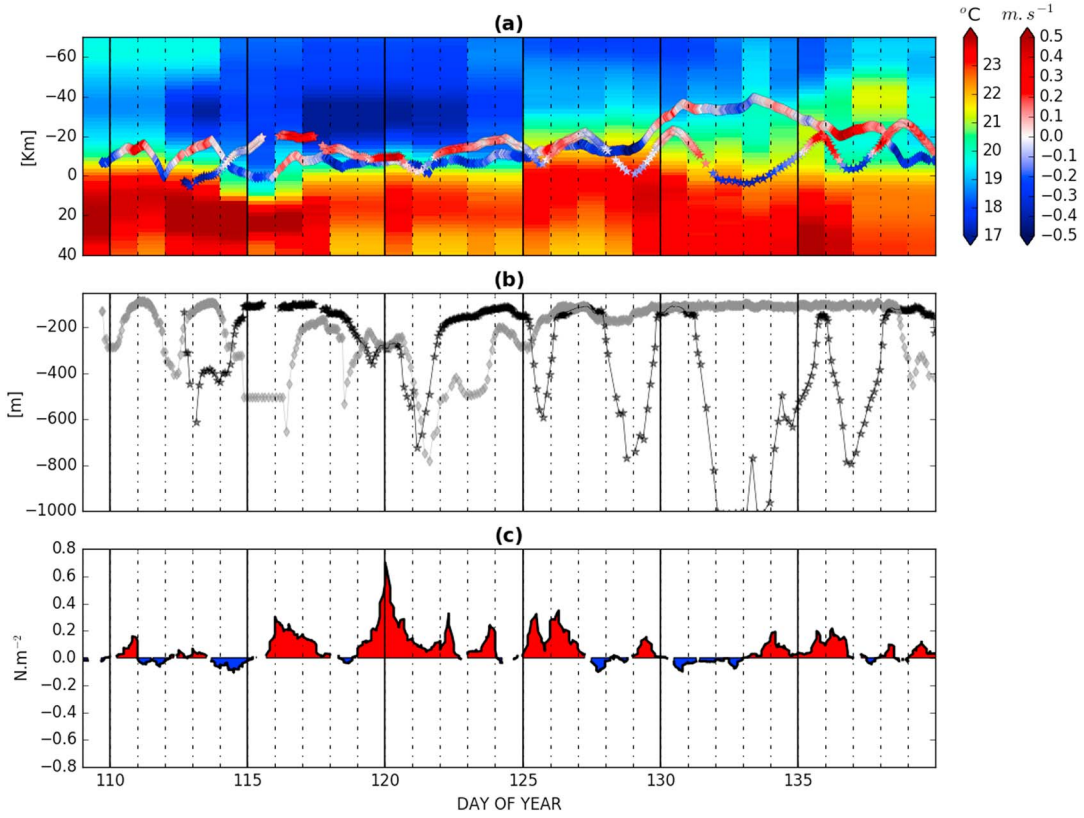

Figure 3. (a) Hovmoller plot of Odyssea SST extracted along 25.75°E. Overlaid are time series of the along-shore depth-averaged currents for SG543 (diamond markers) and SG573 (star markers), with positive velocities (red hues) indicating a flow directed toward the northeast. The *Y* axis represents the distance from the 1000 m isobath with increasing negative values going toward the coast. (b) The black and gray lines show the diving depths for SG543 (diamond markers) and SG573 (star markers), respectively. (c) Along-shore wind stress at 25.75°E, 34.5°S with positive values (red) reflecting upcurrent wind conditions.

radius of about 15 km with maximum surface currents varying between 0.4 m s^{-1} (inshore) and 1.3 m s^{-1} (offshore), resulting in $\zeta = 1.15\ f$ (Figures 2d–2f). Depth-averaged currents displayed maximum speeds of about 0.4 m s^{-1} on both sides of the eddy, as previously. Based on the mean surface velocities measured by SG573 between day 134 and 138, the cyclone propagated southwestward with a phase speed of 37 km d^{-1}.

One more instance of a submesoscale cyclone was observed by SG573 between days 126 and 129 (Figure 3a). All instances of submesoscale cyclones had similar characteristics: They were observed at the AC front, in the regions of strongest topographic and SST gradients (Figures 3a and 3b), had rotation periods of about 2–4 days, and were associated with normalized ζ of order 1, thus pointing to the potential importance of nonlinear and ageostrophic processes.

A cross-shelf representation of the currents over the monthlong record showed a northeastward current at the shelf break, flowing counter to the mean AC direction (Figures 4a and 4c). The region of maximum northeastward flow, located about 20 km inshore of the 1000 m isobath, was coincident with an uplift of ~25 m for the 26.5 kg m^{-3} and 26.8 kg m^{-3} neutral density layers (Figure 4b). The observed northeastward current whose spatial extent and location matched that of the submesoscale eddies most likely represents their cumulative impact on the cross-shelf circulation between days 109 and 140.

3.3. Generation Mechanisms of the Submesoscale Cyclonic Eddies

The dynamical structure of the submesoscale cyclones sampled at the AC inshore front is reminiscent of that observed in larger AC meanders or in other frontal eddies in WBC systems. In the Gulf Stream, the generation mechanism for frontal eddies is a combination of baroclinic and barotropic instability, where the larger mesoscale eddies are formed by mixed baroclinic-barotropic processes [*Gula et al.*, 2015a], and the smaller

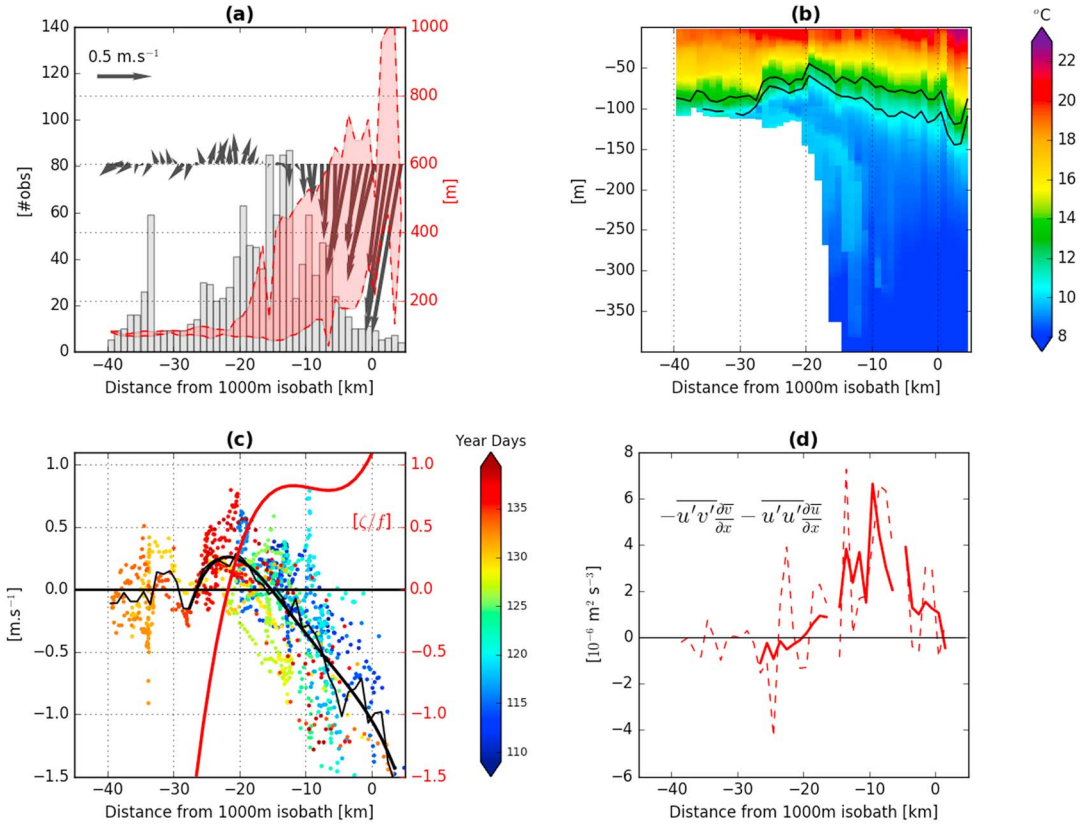

Figure 4. Cross-shelf structure with all parameters averaged in time between year days 109 and 140 and within spatial bins of 1 km. In all panels, the *x* axis represents the distance from the 1000 m isobath in kilometer, with the coastline toward the left-hand side. (a) Vectors show surface currents rotated 45° from north. The histogram shows the number of valid observations with the number counts on the left-hand side *Y* axis. The shaded red area indicates the range of diving depths for the gliders. (b) Vertical cross section of temperature (in °C). Black contour lines in Figure 4b indicate the location of the 26.5 and 26.8 kg m^{-3} neutral density layers (thick line). Note that the CTD data were linearly interpolated along its track in regular 500 m intervals before being bin averaged to prevent spikes in the time-averaged data set. (c) Mean surface along-shore flow (thin black line) and third-order polynomial fit (thick black line). The red line shows the relative vorticity normalized by the Coriolis frequency derived from the fitted shear curve. Colored dots are individual values of along-shore flow with the color bar representing days in 2015. (d) Horizontal shear production term using the along-shore flow mean (dashed line) and fitted mean (plain line).

submesoscale eddies are formed predominantly by barotropic processes in localized areas where the flow interacts with the topography [*Gula et al.,* 2015b].

The AC is remarkably stable between 30°S and 34°S. It is an intense and narrow flow which closely follows the continental slope and is only occasionally disturbed by the passage of mesoscale solitary meanders (about 1.6 times a year on average) [*Rouault and Penven,* 2011]. North of 34°S, *Elipot and Beal* [2015] confirmed that mesoscale solitary meanders could grow by extracting kinetic energy from the mean jet in contrast to the smaller meanders which only caused small offshore excursion in the AC and were not able to extract kinetic energy from the jet to grow.

South of 34°S, the AC behavior changes, and it increasingly meanders. Due to its vertical structure, the AC is more likely to undergo barotropic instability [*De Ruijter et al.,* 1999]. Factors that can affect the growth rate of barotropic instability are the bathymetric curvature and the steepness of the slope. The flow is stabilized when the current is squeezed against the steep slope and becomes unstable when it moves away from the slope due to either bathymetric curvature or the slope becoming less steep [*De Ruijter et al.,* 1999; *Gula et al.,* 2015a]. *Lutjeharms et al.* [2003] noted this tendency for the AC to increasingly meander south of 34° S, where the continental slope widens and the AC moves away from the shelf. Our own analysis of the AC frontal variability using Odyssea SST observations confirms this increase in the meandering of the AC front south of 34°S (supporting information Figure S2). Barotropic instability of the AC likely explains the formation

of mesoscale meanders observed along the Agulhas Bank (so-called frontal or shear-edge eddies) but do not fully explain the presence of submesoscale eddies in a nonmeandering state immediately downstream of Port Elizabeth (34°S).

The steep slope upstream of Port Elizabeth and the AC flowing in its close proximity, with velocities higher than 1.5 m s^{-1}, are favorable conditions for topographic generation of cyclonic vorticity in the bottom boundary layer, as described in *Gula et al.* [2015b]. Considering a shear zone width of a few kilometers, values of relative vorticity several times f can be generated. Strong vorticity generation would lead to horizontal shear instability when the AC separates from the upper slope near 34°S and the formation of submesoscale cyclones. The horizontal scales of the submesoscale cyclones observed during SAGE are identical to the ones formed by horizontal shear instability in the Gulf Stream downstream of the Florida Straits. Thus, the most probable generation mechanism is horizontal shear instability following the sequence of processes described in the Gulf Stream by *Gula et al.* [2015b].

The eddies formed through horizontal shear instability extract their energy from the mean current at a rate given by the horizontal shear production term:

$$\mathrm{HRS} = -\overline{u'v'}\frac{\partial \overline{v}}{\partial x} - \overline{u'u'}\frac{\partial \overline{u}}{\partial x},$$

where the local coordinates are x and y in the cross- and along-shore directions, respectively, and the corresponding horizontal velocities u and v. The overline denotes a time and along-shore mean, and primes the perturbation relative to that mean, such that the total velocities, are written $u = \overline{u} + u'$ and $v = \overline{v} + v'$. For our calculations, the mean and perturbation velocities were computed in spatial bins of 1 km relative to the location of the 1000 m isobath (thick black line in Figure 1) to provide a cross-shelf representation of the time-averaged flow. The conversion from mean to eddy kinetic energy was always positive with a maximum in the region of highest velocity shear. The maximum amplitude $\mathrm{HRS}_{max} = 6.10^{-6}\ \mathrm{m^2\,s^{-3}}$ was comparable to that computed for the Gulf Stream downstream of the Florida Straits ($\mathrm{HRS}_{max} = 1.10^{-5}\ \mathrm{m^2\,s^{-3}}$) [*Gula et al.,* 2015b].

3.4. Formation of Warm Water Plumes Extending Over the Shelf

Warm water shingles extending outward from frontal eddies are frequently observed in the AC [*Lutjeharms,* 2006]. SST imagery collected on day 135 showed the presence of a warm water plume extending toward the shore from the western edge of a cyclone (Figures 2d and 3a). Another instance of a northeastward propagating plume, associated with a cyclone, was observed between days 126 and 129 (Figure 3a). We note here the limitation of merged SST product, which was not able to successfully image this particular plume.

The formation of such plumes is a kinematic effect associated with the cyclones, which advect warm AC water toward the shore [*Lee et al.,* 1981]. What was striking in this instance was that the warm water plumes were moving toward the northeast at speeds exceeding those observed within the cyclones (Figure 3a). Speeds measured within a warm water plume by SG543 between day 134 and 138 reached values of 0.95 m s^{-1} at the surface and 0.68 m s^{-1} for the depth-averaged currents. These were the strongest northeasterly currents recorded during SAGE. In their recent description of a warm water plume associated with a large AC meander, *Pivan et al.* [2016] similarly remarked that the northeasterly velocities observed within the plume exceeded those observed within the AC meander by a factor of 2.

Scant observations of these warm water plumes make it difficult at this stage to determine what drives the strong northeastward flow observed within these features. One explanation could be that local or remote wind forcing drives a northeastward flow on the shelf, which when combined with the inshore cyclonic circulation of the eddies, leads to the formation of a swift northeastward flow near the shelf break.

Wind stress fluctuations during SAGE (Figure 3c) showed that the northeastward motion of the warm plumes could not be attributed to local wind forcing. On day 130 and in the period between days 136 and 138, for example, a warm AC plume propagated swiftly toward the northeast when along-shore winds were weak and variable with a predominantly southwesterly component. Another hypothesis could be that cyclones interact with the continental shelf to excite coastal trapped waves in the form of topographic Rossby waves, which then propagate on the slope with the shallower side on their left in the Southern Hemisphere (i.e., northeastward) [*Louis and Smith,* 1982; *Shaw and Divakar,* 1991].

4. Summary, Perspectives, and Conclusions

WBCs are characterized by a rich submesoscale activity, and small cyclonic eddies have been documented on the flanks of the Loop Current in the Gulf of Mexico [*Rudnick et al.,* 2015] and the Gulf Stream along the South Atlantic Bight [*Gula et al.,* 2015b]. While high-resolution numerical simulations are increasingly highlighting the importance of submesoscale dynamics in the ocean [*Klein et al.,* 2008; *Capet et al.,* 2008; *Gula et al.*, 2016b], in situ observations of submesoscale variability remain elusive. The glider observations collected during SAGE provide the first high-resolution observations of the AC inshore front. Our results show that in a nonmeandering state, the AC current can become unstable due to horizontal shear instability south of 34°S, resulting in the formation of submesoscale cyclones. These submesoscale cyclones are often associated with warm water plumes at their western edge. Current velocities within these warm water plumes were toward the northeast and exceeded those observed in the frontal cyclones.

Over a period of 1 month, we observed a countercurrent at the AC inshore edge, which was associated with an isopycnal uplift of ~25 m. This observed northeast flow likely reveals the intermittent impact of the submesoscale cyclones on the cross-shelf structure. The prevalence of a northeasterly flow at the AC edge could have important consequences for the region as it provides a mechanism for numerous fish species to move eastward and northward against the AC and toward their spawning grounds [*Hutchings et al.,* 2002].

SAGE demonstrates the feasibility and usefulness of ocean gliders to monitor the variability of the AC inshore front. Observations from only two ocean gliders over a period of 1 month allowed us to observe and characterize submesoscale instabilities at the AC inshore edge. However, there is a need to further increase both our spatial and temporal coverage to reduce sampling aliases of these submesoscale features and to improve our understanding of their impact on the coastal and shelf regions.

Acknowledgments

SAGE is a joint research program cofunded by the CSIR-NRE (M. Krug YREF grant EEEO034 and PG grant EEE0023) and SAEON (NRF grant 87306). The data presented in this paper can be requested from the main author and will be made available on the SADCO and NCEI database in 2017. This experiment would not have been possible without the dedication and professionalism shown by oceanographic engineers at Sea Technology Services (STS). In particular, we would like to thank STS engineers Fred Fourie and Jean-Pierre Smit for their invaluable support during deployment and recovery. Many thanks to Tammy Morris from SAEON, the ASCA program, and the crew of the R/V *Algoa* who were instrumental to the successful deployment of the gliders. Thanks to Wayne Goschen, Juliet Hermes, Tommy Bornman, and Shaun Denzel from SAEON for their help throughout the project. Lastly, we would like to thank the numerous technical assistance and advice provided by Geoff Shilling and Craig Lee of the Applied Physics Laboratory, University of Washington. The merged altimetry used to support our results is the DT-MADT "all sat merged" data set produced by Ssalto/Duacs and distributed by AVISO, with support from CNES (http://www.aviso.altimetry.fr/duacs/). The merged Odyssea SST is produced by the CERSAT (http://cersat.ifremer.fr), while the MODIS SST was downloaded from the MRSU website (http://www.afro-sea.org.za). The NCEP Climate Forecast System Version 2 (CFSv2) Selected Hourly Time-Series Products (ds094.1) 10 m winds were downloaded from the NCEP opendap server (http://rda.ucar.edu/datasets/ds094.1/#description). Lastly, we thank the reviewers for their valuable input into this paper.

References

Beal, L. M., and H. L. Bryden (1999), The velocity and vorticity structure of the Agulhas Current at 32°S, *J. Geophys. Res.*, *104*(C3), 5151–5176, doi:10.1029/1998JC900056.

Beal, L. M., W. P. De Ruijter, A. Biastoch, and R. Zahn (2011), On the role of the Agulhas system in ocean circulation and climate, *Nature*, *472*, 429–436.

Brooks, D. A., and J. M. Bane Jr. (1981), Gulf Stream fluctuations and meanders over the Onslow Bay upper continental slope, *J. Phys. Oceanogr.*, *11*(2), 247–256.

Capet, X., J. C. McWilliams, M. J. Molemaker, and A. F. Shchepetkin (2008), Mesoscale to submesoscale transition in the California Current system. Part I: Flow structure, eddy flux, and observational tests, *J. Phys. Oceanogr.*, *38*, doi:10.1175/2007JPO3671.1.

Chelton, D. B., R. A. Deszoeke, M. G. Schlax, K. El Naggar, and N. Siwertz (1998), Geographical variability of the first baroclinic Rossby radius of deformation, *J. Phys. Oceanogr.*, *28*(3), 433–460.

De Ruijter, W. P., P. J. van Leeuwen, and J. R. Lutjeharms (1999), Generation and evolution of Natal Pulses: Solitary meanders in the Agulhas Current, *J. Phys. Oceanogr.*, *29*(12), 3043–3055.

Elipot, S., and L. M. Beal (2015), Characteristics, energetics, and origins of agulhas current meanders and their limited influence on ring shedding, *J. Phys. Oceanogr.*, *45*(9), 2294–2314.

Eriksen, C. C., T. J. Osse, R. D. Light, T. Wen, T. W. Lehman, P. L. Sabin, J. W. Ballard, and A. M. Chiodi (2001), Seaglider: A long-range autonomous underwater vehicle for oceanographic research, *IEEE J. Oceanic Eng.*, *26*(4), 424–436.

Gula, J., M. J. Molemaker, and J. C. McWilliams (2015a), Gulf Stream dynamics along the Southeastern U.S. Seaboard, *J. Phys. Oceanogr.*, *45*, 690–715.

Gula, J., M. J. Molemaker, and J. C. McWilliams (2015b), Topographic vorticity generation, submesoscale instability and vortex street formation in the Gulf Stream, *Geophys. Res. Lett.*, *42*, 4054–4062, doi:10.1002/2015GL063731.

Gula, J., M. J. Molemaker, and J. C. McWilliams (2016a), Submesoscale dynamics of a Gulf Stream frontal eddy in the South Atlantic Bight, *J. Phys. Oceanogr.*, *46*, 305–325.

Gula, J., M. J. Molemaker, and J. C. McWilliams (2016b), Topographic generation of submesoscale centrifugal instability and energy dissipation, *Nat. Commun.*, *7*, 12811.

Hutchings, L., L. E. Beckley, M. H. Griffiths, M. J. Roberts, S. Sundby, and C. Van der Lingen (2002), Spawning on the edge: Spawning grounds and nursery areas around the southern African coastline, *Mar. Freshw. Res.*, *53*(2), 307–318.

Klein, P., B. L. Hua, G. Lapeyre, X. Capet, S. Le Gentil, and H. Sasaki (2008), Upper ocean turbulence from high-resolution 3D simulations, *J. Phys. Oceanogr.*, *38*, 1748–1763.

Krug, M., J. Tournadre, and F. Dufois (2014), Interactions between the Agulhas Current and the eastern margin of the Agulhas Bank, *Cont. Shelf Res.*, *81*, 67–79.

Lee, T. N., L. P. Atkinson, and R. Legeckis (1981), Observations of a Gulf Stream frontal eddy on the Georgia continental shelf, April 1977, *Deep Sea Res.*, *28*(4), 347–378.

Louis, J. P., and P. C. Smith (1982), The development of the barotropic radiation field of an eddy over a slope, *J. Phys. Oceanogr.*, *12*, 56–73.

Lutjeharms, J. R. (2006), *The Agulhas Current*, Springer.

Lutjeharms, J. R. E., R. Catzel, and H. R. Valentine (1989), Eddies and other boundary phenomena of the Agulhas Current, *Cont. Shelf Res.*, *9*(7), 597–616.

Lutjeharms, J. R. E., O. Boebel, and H. T. Rossby (2003), Agulhas cyclones, *Deep Sea Res. II*, *50*(1), 13–34.

Pivan, X., M. Krug, and S. Herbette (2016), Observations of the vertical and temporal evolution of a Natal Pulse along the Eastern Agulhas Bank, *J. Geophys. Res. Oceans*, *121*, 7108–7122, doi:10.1002/2015JC011582.

Rouault, M. J., & Penven P. (2011), New perspectives on Natal Pulses from satellite observations, *J. Geophys. Res.*, *116*, C07013, doi:10.1029/2010JC006866.

Rouault, M. J., A. Mouche, F. Collard, J. A. Johannessen, and B. Chapron (2010), Mapping the Agulhas Current from space: An assessment of ASAR surface current velocities, *J. Geophys. Res.*(1978–2012), *115*, doi:10.1029/2009JC006050.

Rudnick, D. L. (2016), Ocean research enabled by underwater gliders, *Ann. Rev. Mar. Sci.*, *8*, 519–541, doi:10.1146/annurev-marine-122414-033913.

Rudnick, D. L., G. Gopalakrishnan, and B. D. Cornuelle (2015), Cyclonic eddies in the Gulf of Mexico: Observations by underwater gliders and simulations by numerical model, *J. Phys. Oceanogr.*, *45*(1), 313–326 doi:10.1175/JPO-D-14-0138.1.

Saha, S., et al. (2014), The NCEP climate forecast system version 2, *J. Climate*, *27*(6), 2185–2208, doi:10.1175/JCLI-D-12-00823.1.

Schumann, E.H., and I.L. van Heerden, (1988). Observations of the Agulhas Current frontal features south of Africa, October 1983, Deep Sea Res., *35A*, 1355–1362.

Shaw, P. T., and S. Divakar (1991), Generation of topographic waves over the continental margin, *J. Phys. Oceanogr.*, *21*, 1032–1042.

Wong, A., R. Keeley, and T. Carval (2009), Argo quality control manual.

Yelland, M., and P. K. Taylor (1996), Wind stress measurements from the open ocean, *J. Phys. Oceanogr.*, *26*(4), 541–558.